

Supplementary Information on

**Advancing next-generation proton exchange membrane fuel cell design  
through multi-physics and AI modeling**

Guobin Zhang<sup>1</sup>, Zhiguo Qu<sup>1\*</sup>, Qiang Zheng<sup>2</sup>, Yichen Zhou<sup>1</sup>, Ning Wang<sup>1</sup>, Yun Wang<sup>3\*</sup>

1. MOE Key Laboratory of Thermo-Fluid Science and Engineering, School of Energy and Power

Engineering, Xi'an Jiaotong University, Xi'an, Shaanxi 710049, PR China

2. Zhejiang Key Laboratory of Industrial Intelligence and Digital Twin, Eastern Institute of

Technology, Ningbo, Zhejiang 315200, PR China

3. Renewable Energy Resources Lab (RERL), Department of Mechanical and Aerospace

Engineering, University of California, Irvine, CA 92697-3975, United States

\*Corresponding Authors. Tel: +86-29-82668543; E-mail: zgqu@mail.xjtu.edu.cn (Z.G. Qu);

yunw@uci.edu

## 1. Governing equations

The governing equations are listed as below:

Continuity equation (coolant, solved in coolant distribution zones and channels):

$$\frac{\partial \rho_{\text{cool}}}{\partial t} + \nabla \cdot (\rho_{\text{cool}} \mathbf{u}_{\text{cool}}) = 0 \quad \backslash * \text{MERGEFORMAT (1)}$$

Momentum conservation equation (coolant, solved in coolant distribution zones and channels):

$$\frac{\partial}{\partial t} (\rho_{\text{cool}} \mathbf{u}_{\text{cool}}) + \nabla \cdot (\rho_{\text{cool}} \mathbf{u}_{\text{cool}} \mathbf{u}_{\text{cool}}) = -\nabla p_{\text{cool}} + \mu_{\text{cool}} \nabla \cdot (\nabla \mathbf{u}_{\text{cool}}) \backslash *$$

MERGEFORMAT (2)

where  $\rho$  (kg m<sup>-3</sup>),  $\mathbf{u}$  (m s<sup>-1</sup>),  $t$  (s),  $p$  (Pa), and  $\mu$  (Pa s) are the density, velocity, time, pressure, and dynamic viscosity, respectively, and the subscript cool denotes the coolant.

Continuity equation (gas mixture, hydrogen, and water vapor in anode side; oxygen, water vapor and nitrogen in cathode side, solved in anode/cathode gas distribution zones, gas channels, GDLs, MPLs and CLs):

$$\frac{\partial}{\partial t} [\varepsilon(1-s)\rho_g] + \nabla \cdot (\rho_g \mathbf{u}_g) = S_m \quad \text{MERGEFORMAT (3)}$$

Momentum equation (gas mixture flow, i.e., hydrogen and water vapor in anode side; oxygen, water vapor and nitrogen in cathode side, solved in anode/cathode gas distribution zones, gas channels, GDLs, MPLs and CLs):

$$\begin{aligned} \frac{\partial}{\partial t} \left[ \frac{\rho_g \mathbf{u}_g}{\varepsilon(1-s)} \right] + \nabla \cdot \left[ \frac{\rho_g \mathbf{u}_g \mathbf{u}_g}{\varepsilon^2 (1-s)^2} \right] = -\nabla p_g + \mu_g \nabla \cdot \left\{ \nabla \left[ \frac{\mathbf{u}_g}{\varepsilon(1-s)} \right] + \nabla \left[ \frac{\mathbf{u}_g}{\varepsilon(1-s)} \right]^T \right\} \\ - \frac{2}{3} \mu_g \nabla \cdot \left\{ \nabla \cdot \left[ \frac{\mathbf{u}_g}{\varepsilon(1-s)} \right] \mathbf{I} \right\} + \mathbf{S}_u \end{aligned} \quad \text{MERGEFORMAT (4)}$$

MERGEFORMAT (4)

For turbulent flow in headers or other high-Re regions, taking  $k$ - $\varepsilon$  model as an example, turbulent kinetic energy equation:

$$\frac{\partial}{\partial t} (\rho_g k) + \nabla \cdot (\rho_g \mathbf{u}_g k) = \nabla \cdot \left[ \left( \mu_g + \frac{\mu_t}{\sigma_k} \right) \nabla k \right] + G_k - \rho_g \varepsilon \quad \text{MERGEFORMAT (5)}$$

MERGEFORMAT (5)

Turbulent kinetic energy dissipation rate equation:

$$\frac{\partial}{\partial t} (\rho_g \varepsilon) + \nabla \cdot (\rho_g \mathbf{u}_g \varepsilon) = \nabla \cdot \left[ \left( \mu_g + \frac{\mu_t}{\sigma_\varepsilon} \right) \nabla \varepsilon \right] + \frac{c_{\varepsilon 1} \varepsilon}{k} G_k - c_{\varepsilon 2} \rho_g \frac{\varepsilon^2}{k} \quad \text{MERGEFORMAT (6)}$$

MERGEFORMAT (6)

Gas species equation (hydrogen and water vapor in anode side; oxygen, water vapor and nitrogen in cathode side, solved in anode/cathode gas distribution zones, gas channels, GDLs, MPLs and CLs):

$$\frac{\partial}{\partial t} [\varepsilon(1-s)\rho_g Y_i] + \nabla \cdot (\rho_g \mathbf{u}_g Y_i) = \nabla \cdot (\rho_g D_i^{\text{eff}} \nabla Y_i) + S_i \quad \text{\* MERGEFORMAT}$$

MERGEFORMAT (7)

where  $\varepsilon$ ,  $s$ ,  $Y_i$ ,  $D_i^{\text{eff}}$  ( $\text{m}^2 \text{s}^{-1}$ ),  $S_m$  ( $\text{kg m}^{-2} \text{s}^{-2}$ ),  $S_u$  ( $\text{kg m}^{-3} \text{s}^{-1}$ ),  $S_i$  ( $\text{kg m}^{-3} \text{s}^{-1}$ ) are the porosity (which is 1.0 in the distribution zones and flow fields), liquid saturation, species mass fraction, effective diffusion coefficient, source terms of continuity, momentum and gas species equations, respectively, and the subscript g denote gas mixture.

In some models, the liquid water in gas channels is usually described by:

$$\frac{\partial}{\partial t} (\rho_l \varepsilon s) + \nabla \cdot (\rho_l \mathbf{u}_l s) = S_l \quad \text{\* MERGEFORMAT (8)}$$

And the liquid water flow in GDLs, MPLs and CLs are described by:

$$\frac{\partial}{\partial t} (\rho_l \varepsilon s) = \nabla \cdot \left( \rho_l \frac{K k_1}{\mu_l} \nabla p_l \right) + S_l \quad \text{\* MERGEFORMAT (9)}$$

where  $K$  ( $\text{m}^2$ ),  $k_1$ , and  $S_l$  ( $\text{kg m}^{-3} \text{s}^{-1}$ ) are the intrinsic permeability, relative humidity, and source term, respectively.

The water transport in the membrane and CL's ionomer is described by the below governing equation:

$$\frac{\rho_{\text{mem}}}{EW} \frac{\partial}{\partial t} (\omega \lambda) + \nabla \cdot \left( n_d \frac{\mathbf{I}_{\text{ion}}}{F} \right) = \frac{\rho_{\text{mem}}}{EW} \nabla \cdot (D_d^{\text{eff}} \nabla \lambda) + S_{\text{mw}} \quad \text{\* MERGEFORMAT}$$

MERGEFORMAT (10)

where  $\lambda$ ,  $EW$  ( $\text{kg mol}^{-1}$ ),  $\omega$ ,  $n_d$ ,  $\mathbf{I}_{\text{ion}}$ ,  $F$  ( $96,487 \text{ C mol}^{-1}$ ),  $D_d^{\text{eff}}$  ( $\text{m}^2 \text{s}^{-1}$ ) and  $S_{\text{mw}}$  ( $\text{mol}$

$\text{m}^{-3} \text{s}^{-1}$ ) are the membrane water content, equivalent weight of membrane, ionomer volume fraction (1.0 in the membrane), electro-osmotic drag (EOD) coefficient, ionic current density vector, Faraday constant, effective membrane water diffusion coefficient, and source term, respectively.

The electron and proton conductions and the electrochemical reactions are described by a pair of Poisson equations incorporating their reaction rates in the source terms:

$$0 = \nabla \cdot (\kappa_e^{\text{eff}} \nabla \varphi_e) + S_e \quad \backslash * \text{MERGEFORMAT (11)}$$

$$0 = \nabla \cdot (\kappa_{\text{ion}}^{\text{eff}} \nabla \varphi_{\text{ion}}) + S_{\text{ion}} \quad \backslash * \text{MERGEFORMAT (12)}$$

where  $\kappa_{e/\text{ion}}^{\text{eff}}$  ( $\text{S m}^{-1}$ ),  $\varphi_{e/\text{ion}}$  (V), and  $S_{e/\text{ion}}$  ( $\text{A m}^{-3}$ ) are the conductivity, potential, and source term, respectively. The subscripts e and ion denote electron and proton, respectively. The source terms are expressed as:

$$S_e = \begin{cases} -J_a & \text{Anode CL} \\ J_c & \text{Cathode CL} \end{cases}, S_{\text{ion}} = \begin{cases} J_a & \text{Anode CL} \\ -J_c & \text{Cathode CL} \end{cases} \quad \backslash *$$

MERGEFORMAT (13)

where  $J_a$  and  $J_c$  ( $\text{A m}^{-3}$ ) are the hydrogen oxidation reaction (HOR) and oxygen reduction reaction (ORR) rates<sup>[1]</sup>, which can be calculated by the corrected Butler-Volmer equations<sup>[2]</sup>.

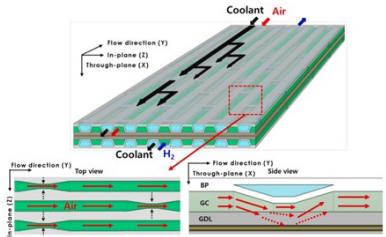
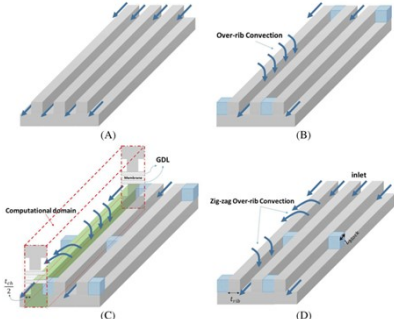
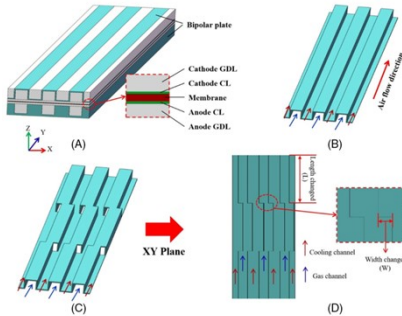
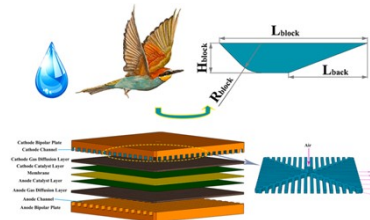
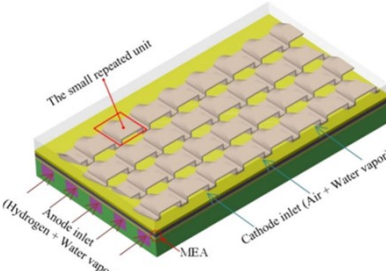
The heat transfer in the whole computational domain is described by the energy conservation equation:

$$\frac{\partial}{\partial t} (\rho^{\text{eff}} C_p^{\text{eff}} T) + \nabla \cdot [\rho^{\text{eff}} C_p^{\text{eff}} \mathbf{u}_g T] = \nabla \cdot (k^{\text{eff}} \nabla T) + S_T \quad \backslash *$$

MERGEFORMAT (14)

where  $T$  (K),  $C_p^{\text{eff}}$  ( $\text{J kg}^{-1}$ ),  $k^{\text{eff}}$  ( $\text{W m}^{-1} \text{K}^{-1}$ ), and  $S_T$  ( $\text{W m}^{-3}$ ) are the temperature, effective heat capacity, effective thermal conductivity, and source term, respectively.

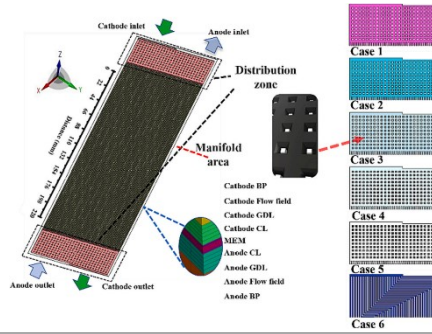
Table S1. Flow field designs by fuel cell multi-physics modeling.

Ref.	Cathode flow field configurations	Flow field type	Active area ( $\text{cm}^2$ )	Distribution zones	Coolant flow
Lim et al. <sup>[3]</sup>		Partially-narrow flow field	3.78	No	Yes
Bagherighajari et al. <sup>[4]</sup>		Interdigitated flow field with block	4.9	No	No
Zhang et al. <sup>[5]</sup>		Staggered channel	3	No	Yes
Xia et al. <sup>[6]</sup>		Bio-inspired channel	4	No	No
Zhang et al. <sup>[7]</sup>		3D fine mesh	0.42	No	No

Zhang et al. <sup>[8]</sup>		Metal foam	0.24	No	No
Valentín-Reyes et al. <sup>[9]</sup>		Interdigitated channel	50	No	No
Atyabi et al. <sup>[10]</sup>		Serpentine channels	100	No	Yes
Sarani et al. <sup>[11]</sup>		Serpentine channels	218	No	Yes
Wang et al. <sup>[12]</sup>		Dot matrix distribution and parallel channels	300	Yes	Yes

Wu et al. <sup>[13]</sup>		Dot matrix distribution and parallel partially-narrow channels	245.76	Yes	Yes
Tsukamoto et al. <sup>[14]</sup>		Dot matrix distribution and parallel channels	300	Yes	Yes
Huo et al. <sup>[15]</sup>		Dot matrix distribution and parallel straight/wave channels	335.4	Yes	Yes
Zhang et al. <sup>[16]</sup>		Bio-inspired channel	3.61	No	No
Zhang et al. <sup>[17]</sup>		Waveform staggered channel	26.95	Yes	Yes
Shao et al. <sup>[18]</sup>		Parallel channel	250	No	No

Lu et al.<sup>[19]</sup>



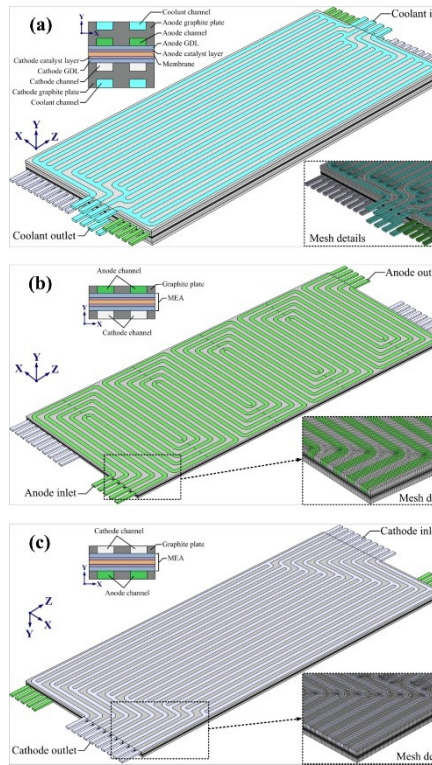
Dot matrix distribution and parallel channels

303.85

Yes

No

Yin et al.<sup>[20]</sup>



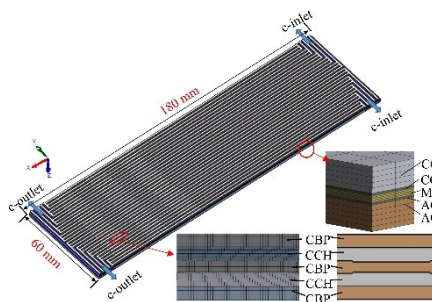
Parallel and serpentine channel

406

No

Yes

Wang et al.<sup>[21]</sup>



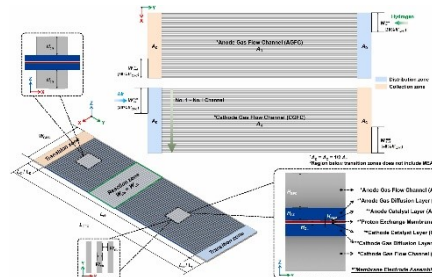
Optimized parallel channel

108

No

No

Wang et al.<sup>[22]</sup>



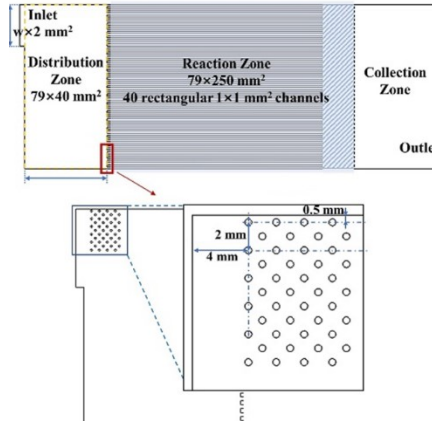
Optimized parallel channel

123.6

Yes

No

Lu et al.<sup>[23]</sup>



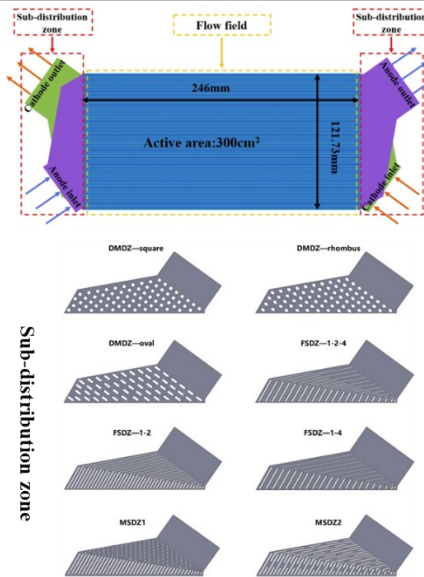
Dot matrix distribution and parallel channels

197.5

Yes

No

Liu et al.<sup>[24]</sup>



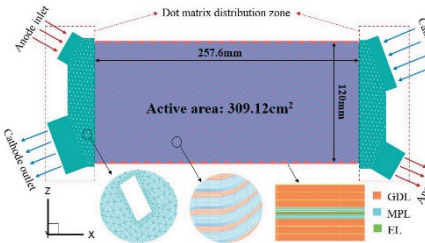
Matrix distribution and parallel channels

300

Yes

No

Huo et al.<sup>[25]</sup>



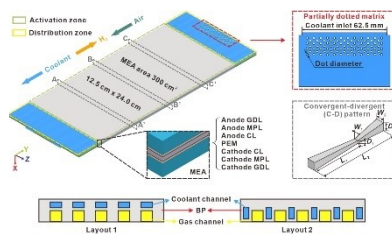
Dot matrix distribution and waveform channels

309.12

Yes

No

Yan et al.<sup>[26]</sup>



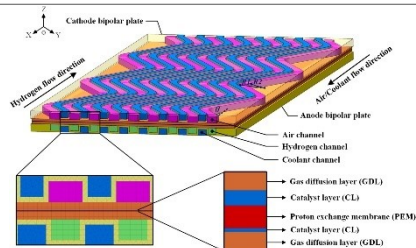
Dot matrix distribution and convergent-divergent flow field

300

Yes

Yes

Liu et al.<sup>[27]</sup>



Wavy flow channel

310

No

Yes

Table S2. Source terms, correlations, and CL agglomerate model parameters

Name	Equations
Source terms in gas continuity equation (kg m <sup>-3</sup> s <sup>-1</sup> )	$S_m = S_{H_2} + S_{O_2} + S_v$
Source terms in gas momentum equation (N m <sup>-3</sup> )	$S_u = -\frac{\mu_g}{Kk_g} \mathbf{u}_g$
Source terms for hydrogen consumption (kg m <sup>-3</sup> s <sup>-1</sup> )	$S_{H_2} = \begin{cases} -\frac{J_a}{2F} M_{H_2} & \text{ACL} \\ 0 & \text{Other zones} \end{cases}$
Source terms for oxygen consumption (kg m <sup>-3</sup> s <sup>-1</sup> )	$S_{O_2} = \begin{cases} -\frac{J_c}{4F} M_{O_2} & \text{CCL} \\ 0 & \text{Other zones} \end{cases}$
Source terms for water vapor transition (kg m <sup>-3</sup> s <sup>-1</sup> )	$S_v = \begin{cases} -S_{v-1} & \text{CHs, GDLs, MPLs} \\ -S_{v-1} + S_{m-v} M_{H_2O} & \text{CLs} \end{cases}$
Leverett-J function (Pa)	$p_c = p_g - p_l = \sigma \cos \theta \left( \frac{\varepsilon}{K} \right)^{0.5} (1.42s - 2.12s^2 + 1.26s^3)$
Source terms in membrane water equation (kg m <sup>-3</sup> s <sup>-1</sup> )	$S_{mw} = \begin{cases} -S_{m-v} - S_p & \text{ACL} \\ -S_{m-v} + S_p + \frac{J_c}{2F} & \text{CCL} \end{cases}$
Liquid pressure permeation source term (kg m <sup>-3</sup> s <sup>-1</sup> )	$S_p = \frac{\rho_l K_{MEM}}{M_{H_2O} \mu_l} \frac{p_l^a - p_l^c}{\delta_{MEM} \delta_{CL}}$
Source terms in energy equation (W m <sup>-3</sup> )	$S_T = \begin{cases}  \nabla \varphi_e ^2 \kappa_e^{\text{eff}} & \text{BPs} \\  \nabla \varphi_e ^2 \kappa_e^{\text{eff}} + S_{v-1} h & \text{GDLs, MPLs} \\ J_a  \eta_{\text{act,con}}^a  +  \nabla \varphi_e ^2 \kappa_e^{\text{eff}} +  \nabla \varphi_{\text{ion}} ^2 \kappa_{\text{ion}}^{\text{eff}} & \text{ACL} \\ + J_a \frac{ \Delta S_a  T}{2F} + (S_{v-1} - S_{m-v}) h & \\ J_c  \eta_{\text{act,con}}^c  +  \nabla \varphi_e ^2 \kappa_e^{\text{eff}} +  \nabla \varphi_{\text{ion}} ^2 \kappa_{\text{ion}}^{\text{eff}} & \text{CCL} \\ + J_c \frac{ \Delta S_c  T}{4F} + (S_{v-1} - S_{m-v}) h & \\  \nabla \varphi_{\text{ion}} ^2 \kappa_{\text{ion}}^{\text{eff}} & \text{Membrane} \\ S_{v-1} h & \text{CHs} \end{cases}$
Typical CL agglomerate model	$J_a = i_{0,a}^{\text{ref}} i_{T,a} a_{\text{Pt,a}}^{\text{eff}} \left( \frac{p_{H_2}}{H_{H_2} C_{H_2}^{\text{ref}}} \right)^{0.5} \left[ \exp \left( \frac{2F \alpha_a}{RT} \eta_{\text{act,con}}^a \right) - \exp \left( -\frac{2F \alpha_c}{RT} \eta_{\text{act,con}}^a \right) \right]$
	$J_c = 4F \frac{p_{O_2}}{H_{O_2}} \left( \frac{1}{E_{\text{agg}} k_c (1 - \varepsilon_{\text{CL}})} + \frac{(r_{\text{agg}} + \delta_m) \delta_m}{a_{\text{agg}} r_{\text{agg}} D_{O_2,N}} \right)^{-1}$

$$k_c = \frac{i_{0,c}^{\text{ref}} a_{\text{Pt,c}}^{\text{eff}} i_{\text{T,c}}}{4F(1-\varepsilon_{\text{CL}})C_{\text{O}_2}^{\text{ref}}} \left[ \exp\left(-\frac{4\alpha_c F}{RT} \eta_{\text{act,con}}^c\right) - \exp\left(\frac{4\alpha_a F}{RT} \eta_{\text{act,con}}^c\right) \right]$$

$$E_{\text{agg}} = \frac{1}{\varphi} \left( \frac{1}{\tanh(3\varphi)} - \frac{1}{3\varphi} \right)$$

$$\varphi = \frac{r_{\text{agg}}}{3} \sqrt{\frac{k_c}{D_{\text{O}_2,\text{N}}^{\text{eff}}}}$$

$$a_{\text{agg}} = \frac{m_{\text{Pt}} \text{ECSA} (1-\varepsilon_{\text{CL}})}{\delta_{\text{CL}} \varepsilon_{\text{Pt/C}}}$$

Table S3. Physical properties and correlations of fuel cell materials

Properties	Values or expressions
Ideal gas constant (J mol <sup>-1</sup> K <sup>-1</sup> )	8.314
Faraday's constant (C mol <sup>-1</sup> )	96487
Gas mixture density (kg m <sup>-3</sup> )	$\rho_g = \frac{p_g}{RT \sum_i \frac{Y_i}{M_i}}$
Gas mixture viscosity (kg m <sup>-1</sup> s <sup>-1</sup> )	$\mu_g = \sum_i Y_i \mu_i$
Effective thermal conductivities (W m <sup>-1</sup> K <sup>-1</sup> )	$k^{\text{eff}} = \varepsilon [s k_1 + (1-s) k_g] + (1-\varepsilon-\omega) k_s + \omega k_{\text{mem}}$
Dynamic viscosity of H <sub>2</sub> , O <sub>2</sub> , H <sub>2</sub> O, and N <sub>2</sub> (kg m <sup>-1</sup> s <sup>-1</sup> )	8.411×10 <sup>-6</sup> , 1.919×10 <sup>-5</sup> , 1.34×10 <sup>-5</sup> , 1.663×10 <sup>-5</sup>
Intrinsic permeability of GDLs, MPLs, CLs, Membrane, and channels (m <sup>2</sup> )	2.0×10 <sup>-12</sup> , 1.0×10 <sup>-12</sup> , 1.0×10 <sup>-13</sup> , 2.0×10 <sup>-20</sup> , 1.0×10 <sup>-8</sup>
Contact angle of GDLs, MPLs, CLs and GDL/CH interface (°)	114, 145, 110, 90
Thermal conductivity of BP, GDL, MPL, CL, and PEM (W m <sup>-1</sup> K <sup>-1</sup> )	20, 2.3, 1, 1, 0.95
Specific heat of BP, GDL, MPL, CL, and PEM (J kg <sup>-1</sup> K <sup>-1</sup> )	1580, 568, 3300, 3300, 833
Density of BP, GDL, MPL, CL, and	1000, 1000, 1000, 1000, 1000

PEM (kg m <sup>-3</sup> )	
Effective ionic conductivity (S m <sup>-1</sup> )	$\kappa_{\text{ion}}^{\text{eff}} = \omega^{1.5} \kappa_{\text{ion}}$
Effective electronic conductivity (S m <sup>-1</sup> )	$\kappa_{\text{e}}^{\text{eff}} = (1 - \varepsilon - \omega)^{1.5} \kappa_{\text{e}}$
Effective species diffusivity (m <sup>2</sup> s <sup>-1</sup> )	$D_i^{\text{eff}} = [\varepsilon (1 - s)]^{1.5} D_i$
Water vapor saturation pressure (atm)	$\log_{10} p_{\text{sat}} = -2.1794 + 0.02953(T - 273.15)$ $- 9.1837 \times 10^{-5} (T - 273.15)^2$ $+ 1.4454 \times 10^{-7} (T - 273.15)^3$

Table S4. Summary of AI integration with multi-physics models.

No.	Authors	Titles	Main contents	Main focuses	Year	AI model
1	Zuo et al. <sup>[28]</sup>	Digital twinning of multi-physics field performance of faceted novel snake coil flow field PEM fuel cells	This study constructs a 3D multiphase multiphysics field digital twin model of a PEMFC using dynamic mode decomposition (DMD), enabling accurate real-time presentation of internal physical fields.	Predict dynamic spatiotemporal evolution in PEM fuel cell	2025	DMD
2	Zhou et al. <sup>[29]</sup>	Machine learning-assisted design of flow fields for proton exchange membrane fuel cells	A depth-first search (DFS) algorithm generates 28,348 flow field designs; 480 are simulated via 3D full-size fuel cell model to create a training dataset. A multilayer perceptron (MLP) model then predicts current density from flow field morphology, enabling rapid screening of high-performance designs to identify the optimal flow field structure.	Optimization of flow field structure	2025	DFS, MLP
3	Alibeigi et al. <sup>[30]</sup>	Integrated study of prediction and optimization performance of PBI-HTPEM fuel cell using deep learning, machine learning and statistical correlation	3D full-size modeling and AI methods are used to predict and optimize the performance of PBI-HTPEM fuel cells, comparing various machine learning techniques and metaheuristic algorithms for maximizing power and current density with low errors and computational cost.	Optimization of operation conditions	2024	SVR, GPR, FC-NN
4	Ghasabehi and Shams <sup>[31]</sup>	Predicting water saturation and oxygen transport resistance in proton exchange membrane fuel cell by	This work develops a hybrid "3D+1D" PEMFC model, where 3D domain simulates two-phase flow and a simplified 1D domain handles electrochemical processes. Machine learning predicts water saturation and oxygen transport resistance trained by the dataset from 3D fuel cell model, which bridges	Prediction of water saturation and oxygen transport	2024	CatBoost algorithm, etc.

		artificial intelligence	flow-field characteristics with flooding behavior, enabling efficient integration into the hybrid framework for accurate flood prediction	resistance, construction of a cost-effective 3D+1D model		
5	Ghasabehi et al. <sup>[32]</sup>	Optimization of baffle and tapering integration in the PEM fuel cell flow field employing artificial intelligence	This study employs AI to develop surrogate models for optimizing the integration of baffles and tapering in flow fields, achieving superior accuracy in enhancing performance and output power density.	Optimization of operation conditions and geometry	2024	FC-NN
6	Pan et al. <sup>[33]</sup>	A machine learning driven 3D+1D model for efficient characterization of proton exchange membrane fuel cells	This study presents a computationally efficient AI-driven 3D+1D model, where the AI surrogate reduces the computational intensity of the 1D electrochemical sub-model while maintaining high accuracy.	Partially replace some parts in 3D full-size fuel cell model	2024	FC-NN
7	Srivastava et al. <sup>[34]</sup>	A non-intrusive approach for physics-constrained learning with application to fuel cell modeling	This study introduces weakly-coupled Integrated Inference and Machine Learning (IIML) framework that improves physical model accuracy by inferring and correcting model structures.	Calibration of model parameters for improving accuracy	2023	FC-NN
8	Nguyen et al. <sup>[35]</sup>	Deep learning-based optimization of a microfluidic membraneless fuel cell for maximum power density via data-driven three-dimensional multi-physics	This study introduces a deep learning-based method combining ANN and GA to optimize a membraneless microfluidic fuel cell for maximum power density using 3D multi-physics simulation data.	Optimization of geometry	2022	FC-NN, GA

		simulation data				
9	Lou et al. <sup>[36]</sup>	Machine-learning-assisted insight into the cathode catalyst layer in proton exchange membrane fuel cells	This study integrates the Extreme Gradient Boosting (XGBoost) machine learning algorithm with a 3D full-size fuel cell model to analyze and optimize the CL. The data-driven model uses the 3D model to generate training datasets for rapid prediction of cell performance, quantitative sensitivity analysis, and multi-objective optimization via GA	Sensitivity analysis and Optimization of CL composition parameters	2022	XGBoost, GA
10	Tian et al. <sup>[37]</sup>	Deep learning from three-dimensional multiphysics simulation in operational optimization and control of polymer electrolyte membrane fuel cell for maximum power	Using 3D full-size model to generate dataset, this paper proposes an ANN model to predict fuel cell's performance rapidly and then integrates it with GA to identify the maximum power at different application temperatures	Optimization of operation conditions	2021	FC-NN, GA
11	Zhang et al. <sup>[38]</sup>	Optimization of porous media flow field for proton exchange membrane fuel cell using a data-driven surrogate model	Using 3D full-size model to generate dataset, this paper proposes a SVM model to predict fuel cell's performance rapidly and then integrates it with GA to identify the optimal porous flow field structure corresponding to the maximum performance of fuel cells	Optimization of geometry of porous flow field	2020	SVM, GA
12	Li et al.	Performance prediction and power density maximization of a proton exchange membrane fuel cell based on deep belief network	This paper employs a deep belief network (DBN) to construct a data-driven model for predicting PEMFC performance and maximizing power density	Optimization of operation conditions	2020	DBN

13	Wang et al. <sup>[39]</sup>	Multi-physics-resolved digital twin of proton exchange membrane fuel cells with a data-driven surrogate model	This paper presents a surrogate modelling method that integrates a 3D fuel cell physical model with a data-driven model, leveraging AI to efficiently predict multi-physics fields, reduce computational cost, and enable development of digital twins for complex systems.	Prediction of spatial distributions of multiple flow fields	2020	FC-NN, SVM
14	Wang et al. <sup>[40]</sup>	AI-based optimization of PEM fuel cell catalyst layers for maximum power density via data-driven surrogate modeling	Using a 3D full-size model to generate dataset, this paper proposes a SVM model to quickly predict fuel cell performance and then integrates it with GA to identify the optimal CL composition corresponding to the maximum power density of fuel cells	Optimization of CL composition parameters	2020	SVM, GA

## References

- [1] Kong Z, Wu J, Liu Z, Yan D, Wu ZP, Zhong CJ. Advanced electrocatalysts for fuel cells: Evolution of active sites and synergistic properties of catalysts and carrier materials. *Exploration*, 2025,5(1):20230052.
- [2] Zhang G, Wu J, Wang Y, Yin Y, Jiao K. Investigation of current density spatial distribution in PEM fuel cells using a comprehensively validated multi-phase non-isothermal model. *International Journal of Heat and Mass Transfer*, 2020,150:119294.
- [3] Lim K, Kim C, Park R, Alam A, Ju H. Enhancing PEMFC performance through orifice-shaped cathode flow field designs: A multiscale, multiphase simulation study on oxygen supply and water removal. *Chemical Engineering Journal*, 2023,475.
- [4] Bagherighajari F, Ramiar A, Abdollahzadehsangroudi M, Páscoa JC, Oliveira PJ. Numerical simulation of the polymer electrolyte membrane fuel cells with intermediate blocked interdigitated flow fields. *International Journal of Energy Research*, 2022,46(11):15309-31.
- [5] Zhang Z, Wang C, Chen C. Numerical study on the effect of a novel staggered flow field on the performance of proton exchange membrane fuel cell. *International Journal of Energy Research*, 2022,46(13):18648-62.
- [6] Xia L, Yu Z, Xu G, Ji S, Sun B. Design and optimization of a novel composite bionic flow field structure using three-dimensional multiphase computational fluid dynamic method for proton exchange membrane fuel cell. *Energy*

- Conversion and Management, 2021,247:114707.
- [7] Zhang G, Xie B, Bao Z, Niu Z, Jiao K. Multi-phase simulation of proton exchange membrane fuel cell with 3D fine mesh flow field. *International Journal of Energy Research*, 2018,42(15):4697-709.
- [8] Zhang G, Bao Z, Xie B, Wang Y, Jiao K. Three-dimensional multi-phase simulation of PEM fuel cell considering the full morphology of metal foam flow field. *International Journal of Hydrogen Energy*, 2021,46(3):2978-89.
- [9] Valentín-Reyes J, León MI, Pérez T, Romero-Castañón T, Beltrán J, Flores-Hernández JR, Nava JL. Simulation of an interdigitated flow channel assembled in a proton exchange membrane Fuel Cell (PEMFC). *International Journal of Heat and Mass Transfer*, 2022,194:123026.
- [10] Atyabi SA, Afshari E, Udemu C. Comparison of active and passive cooling of proton exchange membrane fuel cell using a multiphase model. *Energy Conversion and Management*, 2022,268:115970.
- [11] Sarani I, Xie B, Bao Z, Huo W, Li X, Xu Y, Wang B, Jiao K. Analysis of phase change material thermal effects in large-scale proton-exchange membrane fuel cell based on open-source computational fluid dynamics. *Applied Thermal Engineering*, 2022,216:119143.
- [12] Wang N, Qu Z, Zhang G, Tang Z, Wang Y. Cross flow and distribution characteristics in automobile polymer electrolyte membrane fuel cells: A three-dimensional full-scale modeling study. *Journal of Power Sources*, 2023,580:233348.

- [13] Wu L, Zhang G, Shi X, Pan Z, Xie B, Huo W, Jiao K, An L. All-scale investigation of a commercial proton exchange membrane fuel cell with partially narrow channels. *Journal of Power Sources*, 2024,589:233779.
- [14] Tsukamoto T, Aoki T, Kanesaka H, Taniguchi T, Takayama T, Motegi H, Takayama R, Tanaka S, Komiyama K, Yoneda M. Three-dimensional numerical simulation of full-scale proton exchange membrane fuel cells at high current densities. *Journal of Power Sources*, 2021,488:229412.
- [15] Huo W, Liu B, Xu W, Xie B, Fan L, Benbouzid M, Xu Y, Ding T, Fang C, Gao F, Amirat Y, Li F, Jiao K. High precision and efficient simulation of large-size proton exchange membrane fuel cells incorporated with a novel alternative cooling method. *International Journal of Heat and Mass Transfer*, 2024,230:125780.
- [16] Zhang S, Liu S, Xu H, Liu G, Wang K. Performance of proton exchange membrane fuel cells with honeycomb-like flow channel design. *Energy*, 2022,239:122102.
- [17] Yong Z, Shirong H, Xiaohui J, Yuntao Y, Mu X, Xi Y. Characteristics of proton exchange membrane fuel cell considering “dot matrix” gas distribution zones and waveform staggered flow field with cooling channels. *Energy Conversion and Management*, 2022,267:115881.
- [18] Shao H, Qiu D, Peng L, Yi P, Lai X. In-situ measurement of temperature and humidity distribution in gas channels for commercial-size proton exchange membrane fuel cells. *Journal of Power Sources*, 2019,412:717-24.

- [19] Lu G, Liu M, Su X, Zheng T, Luan Y, Fan W, Cui H, Liu Z. Study on counter-flow mass transfer characteristics and performance optimization of commercial large-scale proton exchange membrane fuel cells. *Applied Energy*, 2024,359:122743.
- [20] Yin C, Cao J, Tang Q, Su Y, Wang R, Li K, Tang H. Study of internal performance of commercial-size fuel cell stack with 3D multi-physical model and high resolution current mapping. *Applied Energy*, 2022,323:119567.
- [21] Wang Y, Guan C, Li H, Zhao Y, Wang C, He W. Flow field configuration design for a large-scale hydrogen polymer electrolyte membrane fuel cell. *Applied Energy*, 2023,351:121852.
- [22] Wang B, Pan W, Hu Z, Zhang G, Tang L, Chen X, Wang F. Comprehensive investigation on impacts of flow uniformity on performance of large-scale PEM fuel cells. *Energy*, 2025,332:137039.
- [23] Lu W, Pan W, Chen Z, Gao Y, Ding L, Chen X, Wang F. Structural optimization of distribution zone for large-sized PEMFC with high power density. *Chemical Engineering Science*, 2023,276.
- [24] Liu B, Huo W, Xie B, Gao Q, Bao Z, Li H, Wu K, He S, Du Q, Qin B, Jiao K. Effects of sub-distribution zone structure of bipolar plate on the mass transport of large-area proton exchange membrane fuel cells. *International Journal of Heat and Mass Transfer*, 2024,222.
- [25] Huo W, Xie B, Wu S, Wu L, Zhang G, Zhang H, Qin Z, Zhu Y, Wang R, Jiao K. Full-scale multiphase simulation of automobile PEM fuel cells with different

- flow field configurations. *International Journal of Green Energy*, 2023,21(1):154-69.
- [26] Yan C, Zeng Z, Tao X, Zhang W, Guan C, Sun K, Che Z, Wang T. Coupling study of large-scale commercial proton exchange membrane fuel cell with novel convergent-divergent flow field and multiple coolant flow fields. *Applied Thermal Engineering*, 2025,278:127363.
- [27] Liu Q, Zhao Z, Lin Z, Wang H, Yuan Y. Study on the power performance improvement of a large-scale proton exchange membrane fuel cell stack with novel wavy flow channels. *Energy Conversion and Management*, 2025,342:120127.
- [28] Zuo Q, Wang G, Shen Z, Zhu X, Xie Y, Li Y, Ma Y, Zhang H. Digital twinning of multi-physics field performance of faceted novel snake coil flow field proton exchange membrane fuel cells. *Journal of Power Sources*, 2025,649:237442.
- [29] Zhou X, Zhang J, Feng K, Qiao Z, Wang Y, Shi L. Machine learning-assisted design of flow fields for proton exchange membrane fuel cells. *Journal of Power Sources*, 2025,626:235753.
- [30] Alibeigi M, Jazmi R, Maddahian R, Khaleghi H. Integrated study of prediction and optimization performance of PBI-HTPEM fuel cell using deep learning, machine learning and statistical correlation. *Renewable Energy*, 2024,235:121295.
- [31] Ghasabehi M, Shams M. Predicting water saturation and oxygen transport resistance in proton exchange membrane fuel cell by artificial intelligence. *Fuel*,

2024,368:131557.

- [32] Ghasabehi M, Ghanbari S, Asadi MR, Shams M, Kanani H. Optimization of baffle and tapering integration in the PEM fuel cell flow field employing artificial intelligence. *Energy*, 2024,302:131884.
- [33] Pan Y, Ruan H, Wu B, Regmi YN, Wang H, Brandon NP. A machine learning driven 3D+1D model for efficient characterization of proton exchange membrane fuel cells. *Energy and AI*, 2024,17:100397.
- [34] Srivastava V, Sulzer V, Mohtat P, Siegel JB, Duraisamy K. A non-intrusive approach for physics-constrained learning with application to fuel cell modeling. *Computational Mechanics*, 2023,72(2):411-30.
- [35] Nguyen DD, Quy Duc Pham T, Tanveer M, Khan H, Park JW, Park CW, Kim GM. Deep learning-based optimization of a microfluidic membraneless fuel cell for maximum power density via data-driven three-dimensional multiphysics simulation. *Bioresource Technology*, 2022,348:126794.
- [36] Lou Y, Hao M, Li Y. Machine-learning-assisted insight into the cathode catalyst layer in proton exchange membrane fuel cells. *Journal of Power Sources*, 2022,543:231827.
- [37] Tian P, Liu X, Luo K, Li H, Wang Y. Deep learning from three-dimensional multiphysics simulation in operational optimization and control of polymer electrolyte membrane fuel cell for maximum power. *Applied Energy*, 2021,288:116632.
- [38] Zhang G, Wu L, Jiao K, Tian P, Wang B, Wang Y, Liu Z. Optimization of

porous media flow field for proton exchange membrane fuel cell using a data-driven surrogate model. *Energy Conversion and Management*, 2020,226:113513.

- [39] Wang B, Zhang G, Wang H, Xuan J, Jiao K. Multi-physics-resolved digital twin of proton exchange membrane fuel cells with a data-driven surrogate model. *Energy and AI*, 2020,1:100004.
- [40] Wang B, Xie B, Xuan J, Jiao K. AI-based optimization of PEM fuel cell catalyst layers for maximum power density via data-driven surrogate modeling. *Energy Conversion and Management*, 2020,205:112460.